

## Measurement of tensor analyzing powers in deuteron photodisintegration.

I.A.Rachek,<sup>1</sup> L.M.Barkov,<sup>1</sup> S.L.Belostotsky,<sup>2</sup> V.F.Dmitriev,<sup>1</sup> M.V.Dyug,<sup>1</sup> R.Gilman,<sup>3</sup> R.J. Holt,<sup>4</sup> B.A.Lazarenko,<sup>1</sup> S.I.Mishnev,<sup>1</sup> V.V.Nelyubin,<sup>2</sup> D.M.Nikolenko,<sup>1</sup> A.V.Osipov,<sup>5</sup> D.H. Potterveld,<sup>4</sup> R.Sh.Sadykov,<sup>1</sup> Yu.V.Shestakov,<sup>1</sup> V.N.Stibunov,<sup>5</sup> D.K.Toporkov,<sup>1</sup> H.de Vries,<sup>6</sup> and S.A.Zevakov<sup>1</sup>

<sup>1</sup>*Budker Institute of Nuclear Physics, 630090 Novosibirsk, Russia*

<sup>2</sup>*Saint-Petersburg Institute of Nuclear Physics, 188350 Gatchina, Russia*

<sup>3</sup>*Rutgers University, Piscataway, NJ 08855, USA*

<sup>4</sup>*Argonne National Laboratory, Argonne, IL 60439, USA*

<sup>5</sup>*Institute of Nuclear Physics at Tomsk Polytechnic University, 634050 Tomsk, Russia*

<sup>6</sup>*NIKHEF, P.O.Box 41882, 1009 DB Amsterdam, The Netherlands*

(Dated: January 24, 2007)

A new accurate measurement of the tensor analyzing powers  $T_{20}$ ,  $T_{21}$  and  $T_{22}$  in deuteron photodisintegration has been performed. Wide-aperture non-magnetic detectors allowed broad kinematic coverage in a single setup:  $E_\gamma = 25$  to 600 MeV, and  $\theta_p^{cm} = 24^\circ$  to  $48^\circ$  and  $70^\circ$  to  $102^\circ$ . The new data provide a significant improvement over the few existing measurements. The angular dependency of the tensor asymmetries in deuteron photodisintegration is extracted for the first time.

PACS numbers: 24.70.+s, 24.20.-x

The simplest nucleus, the deuteron, is a natural laboratory for the study of nuclear forces. One of the most fundamental processes on the deuteron is two-body photodisintegration (PD)  $\gamma + d \rightarrow p + n$ . It has been a subject of intensive experimental and theoretical research for over 70 years (see Ref. [1] for a comprehensive review). However several important observables still are measured with insufficient accuracy or not measured at all. The tensor analyzing powers accessible through measurement of target asymmetries in PD of tensor polarized deuteron are among the most poorly known. Polarization observables are expected to be sensitive to important dynamical details and thus allow in general much more stringent tests of theoretical models. The tensor polarizations are especially interesting because there is a correlation between the degree of tensor polarization and the spatial alignment of the deuteron. For example, spatial alignment of the target deuterons can lead to large asymmetries from final state interactions in PD.

A general expression for the cross-section of the two-body PD of the polarized deuteron is written as follows:

$$\frac{d\sigma}{d\Omega} = \frac{d\sigma_0}{d\Omega} \left\{ 1 - \sqrt{3/4} P_z \sin \theta_H \sin \phi_H T_{11} + \sqrt{1/2} P_{zz} \left[ (3/2 \cos^2 \theta_H - 1/2) T_{20} - \sqrt{3/8} \sin 2\theta_H \cos \phi_H T_{21} + \sqrt{3/8} \sin^2 \theta_H \cos 2\phi_H T_{22} \right] \right\}, \quad (1)$$

with  $\sigma_0$  the unpolarized cross-section,  $P_z$  ( $P_{zz}$ ) the degree of vector (tensor) polarization of the target,  $\theta_H$  the angle between polarization axis and momentum of  $\gamma$ -quantum, and  $\phi_H$  the angle between the polarization plane (containing the polarization axis and momentum of the photon) and the reaction plane (containing momenta of the proton and neutron). The tensor analyzing powers  $T_{2I}$  are functions of photon energy  $E_\gamma$  and proton emission angle  $\theta_p^{cm}$ .

Only three measurements of tensor polarization observables in deuteron PD have been reported prior to this experi-

ment [2–4]. Here we present the results of a new measurement of the tensor analyzing power components  $T_{20}$ ,  $T_{21}$  and  $T_{22}$ .

The measurements were performed at the 2 GeV electron storage ring VEPP-3. A thin-wall open-ended storage cell fed by polarized deuterium gas from an Atomic Beam Source (ABS) was used as an internal target [5]. The ABS provides a polarized deuterium gas jet with an intensity of up to  $8 \times 10^{16}$  atoms/s and a very high degree of tensor polarization – above 98% from extreme values (+1 or –2), while vector polarization was always close to zero ( $|P_z| < 0.02$ ). Polarization of the gas stored inside the cell is degraded due to various depolarizing processes. The target polarization was determined by the “Low-Q” polarimeter [6]. Tensor polarization averaged over the whole run of data taking was found to be  $P_{zz}^+ = 0.341 \pm 0.025 \pm 0.011$ , where the first uncertainty is statistical and the second one is systematic. The ratio  $P_{zz}^-/P_{zz}^+ = -1.70 \pm 0.15$  is obtained by the analysis of the data collected on polarized and unpolarized deuterium target.

In this experiment we measured the counting rate asymmetry for two signs of tensor polarization of the deuterium target in disintegration of the deuteron by a 2-GeV electron scattered forward, i.e. at an angle  $\vartheta_e \approx 0^\circ$ . In final state we detect the proton and neutron in coincidence, the scattered electron is not detected. Scattering of an electron at  $0^\circ$  is equivalent to the radiation of a real photon, which is then absorbed by a deuteron – that is why in such a set-up it is the *photo*-disintegration, that is studied.

During the run the polarization settings were switched every 30 seconds to suppress systematic uncertainties. It takes less than a second to alternate the polarization by changing a resonance magnetic field in the rf-transition unit, located inside the ABS. The experimental tensor target asymmetry is defined as

$$a^T = \sqrt{2}(N^+ - N^-)/(P_{zz}^+ N^- - P_{zz}^- N^+), \quad (2)$$

where  $N^+$  ( $N^-$ ) denotes the number of events detected with positive (negative) target polarization.

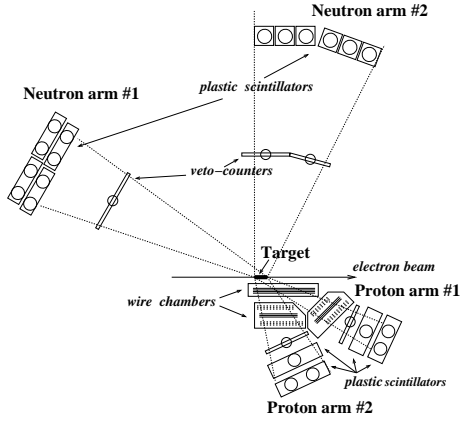


FIG. 1: Schematic side view of the particle detectors.

In order to disentangle the three components of tensor analyzing power we collected data for three settings of the magnetic field, defining the polarization axis:  $\theta_{H0} = 0^\circ$ ,  $\theta_{H1} = 54.7^\circ$  and  $\theta_{H2} = 125.3^\circ$ , with  $\phi_H$  close to  $0^\circ$  for all settings. According to Eq. 1 the target asymmetry in these cases is proportional to  $a_0^T \sim c_0 T_{20}$ ,  $a_1^T \sim (-c_1 T_{21} + c_2 T_{22})$  and  $a_2^T \sim (+c_1 T_{21} + c_2 T_{22})$  respectively. Here  $c_0, c_1, c_2$  are constants defined by a geometry of detector and target. Therefore all three tensor moments are separated unambiguously. Note that a term with  $T_{11}$  is suppressed in all three configurations even for non-zero vector polarization  $P_z$  due to its  $\sin \phi$ -dependence, see Eq. 1.

The particle detector consists of two pairs of arms for detecting protons and neutrons in coincidence, as shown in Fig. 1. The first (second) pair covers an angle range of  $\theta_p^{cm} = 24^\circ$  to  $48^\circ$  ( $\theta_n^{cm} = 70^\circ$  to  $102^\circ$ ). Each proton arm includes wire chambers for tracking and 3 layers of plastic scintillators (2 + 12 + 12cm thick). Neutron arms consist of plastic scintillators: 2-cm charged particle veto counters followed by 20-cm or 12 + 12cm scintillator bars placed at a largest available distance from the target, about 3 m, for the best TOF measurement. Azimuthal angular acceptance was  $\Delta\varphi = 20^\circ$  for all arms.

Particle identification was based on the veto signal and TOF analysis for neutrons and on TOF and  $\Delta E/E$  analysis for protons. Further event selection relies on kinematic correlations characteristic of the two-body PD – see Fig 2a–c. One such property is a coplanarity of proton and neutron momenta ( $|\phi_p - \phi_n| = \pi$ ). Assuming deuteron two-body disintegration by a photon emitted along the electron beam direction, one can reconstruct  $E_\gamma$  and cm angles from the momentum vector of a single detected proton or neutron. This provides two more selection criteria:  $E_\gamma^{(p)} = E_\gamma^{(n)}$  and  $\vartheta_p^{cm} + \vartheta_n^{cm} = \pi$ . Such cuts allow both to reject the background and to constrain the electron scattering angle to  $\vartheta_e < 0.5^\circ \dots 2.0^\circ$ , depending on  $E_\gamma$ . An amount of inseparable residual background, which comes mostly from three-body PD  $d(\gamma, pn)\pi^0$ , was estimated from the analysis of a tail in the out-of-plane events distribution. The shape of the tail is determined by selecting the events of a similar 3-body disintegration process  $d(\gamma, pp)\pi^-$

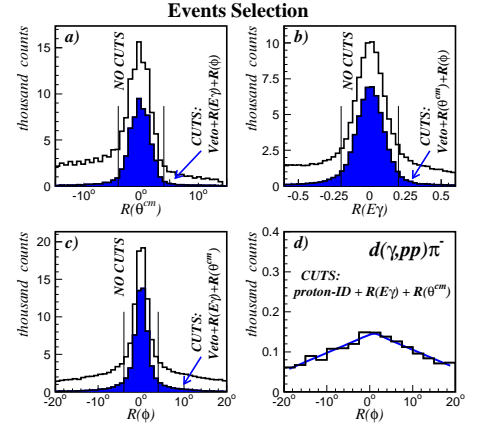


FIG. 2: Selection of two-body deuteron PD events. Panels a)–c) are histograms of correlation parameters:  $R(\vartheta^{cm}) = \vartheta_p^{cm} - \vartheta_n^{cm} - \pi$ ,  $R(E_\gamma) = (E_\gamma^{(p)} - E_\gamma^{(n)}) / ((E_\gamma^{(p)} + E_\gamma^{(n)}) / 2)$ ,  $R(\varphi) = \varphi_p - \varphi_n - \pi$ . Shaded histograms are for all cuts applied except the cut on the shown parameter. Vertical lines indicate the cut on the shown parameter. Panel d) shows a shape of out-of-plane events distribution for the three-body deuteron disintegration, which is selected by identifying a proton in the neutron arm using TOF/E and  $\Delta E/E$  analysis.

– see Fig 2d. The background analysis was performed separately for each polarization state. After applying all cuts the fraction of unseparated background events was estimated to be from 1.5% (low  $E_\gamma$  region) to 5.6% (high  $E_\gamma$  region). The uncertainty from the unseparated background events is included in the statistical uncertainty.

The main source of systematic uncertainty is the uncertainty in the target polarization. The degree of polarization enters as a common factor for all data points. Other systematic uncertainties come from the inaccuracy of reconstruction of  $E_\gamma$  and proton CM–emission angle. Contribution of these parameters dominates at small  $E_\gamma$  where tensor analyzing powers change fast with energy. The false asymmetry related to fluctuations of other experimental parameters, such as electron beam lifetime, target density variations, PMT gain instability, etc is negligible because these fluctuations were completely unsynchronized with the reversing of polarization, and characteristic time of fluctuations was much higher than the period of reversing of polarization (30 s). Moreover, the beam current integral and time spent in each polarization state were measured precisely and taken into account in the analysis.

In Figures 4,5 systematic errors are presented as shaded bands at top or bottom of the plots.

Tensor analyzing powers are functions of two variables, and usually  $E_\gamma^{lab}$  and  $\vartheta_p^{cm}$  are chosen. Our data cover substantially broad continuous regions of both variables. Binning of the experimental data was done in order to provide both sufficient statistical precision and a reasonable number of bins to display the dependence of tensor moments on kinematic variables.

To compare the new data with the results of earlier measurements [4], a subset of the data, where the kinematic acceptances of two measurements overlap, was selected[12] –

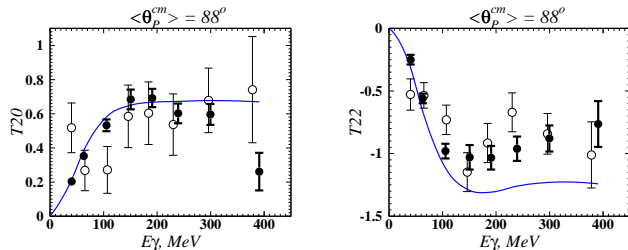


FIG. 3: Comparison of previous data [4] (open circles) and this work (filled circles). Only the part of the new data which corresponds to the kinematic conditions of the previous measurement is shown. Theoretical curve is the full calculation from [7]

see Fig. 3. One can see that two measurements are consistent within uncertainties.

To compare the data to theoretical predictions we have performed an event weighted averaging of the theory over the phase-space of each experimental bin. The calculation [7] starts from a one-body current using the Bonn OBEPR  $NN$  potential with the major part of meson exchange currents (MEC) included implicitly via the Siegert operators; this model is denoted as "normal" (N). Then explicit pion exchange currents ("+MEC"), isobar configurations ("+IC") and the leading order relativistic corrections ("+RC") are added successively. The calculation of [8] was done in a diagrammatic approach with all MEC, including heavy-meson ones, introduced explicitly, and isobar configurations and relativistic corrections added. This calculation is restricted to  $E_\gamma$  below pion production threshold. In [9] the deuteron PD beyond pion production threshold is studied in a coupled-channel approach including  $N\Delta$  and  $\pi d$  channels, with the dynamical treatment of the pion. In consequence the  $NN$  potential and  $\pi$ -MEC become retarded and electromagnetic loop corrections have been incorporated. In [10] this concept was further elaborated and numerical results for various observables were obtained.

The dependence of tensor analyzing powers on  $E_\gamma$  is plotted in Fig. 4. Here the whole dataset is divided into two  $\theta_p^{cm}$  bins, each related to the data from one pair of detector arms. Alternately, in Fig 5 the tensor moments versus  $\theta_p^{cm}$  are shown for eight  $E_\gamma$ -bins. The numerical results are available from [11].

Figures 4 and 5 show that up to about pion production threshold, there is little variation between the theoretical calculations [7, 8], and there is good agreement between these calculations and the data. The most noticeable difference is that  $T_{22}$  tends to be slightly more positive than calculated. Above pion production, the calculations become significantly more complex due to the larger effects of relativity and the increasing importance of additional channels, as the pion can propagate on-shell, and the energy approaches the  $\Delta$  resonance region. We see greater variations between the older calculation of [7] and the more modern calculation of [10]. The more modern calculations improve the description of  $T_{20}$  and  $T_{22}$ , but do worse for  $T_{21}$ . Despite the disagreement in details, it is clear that there is a good overall qualitative descrip-

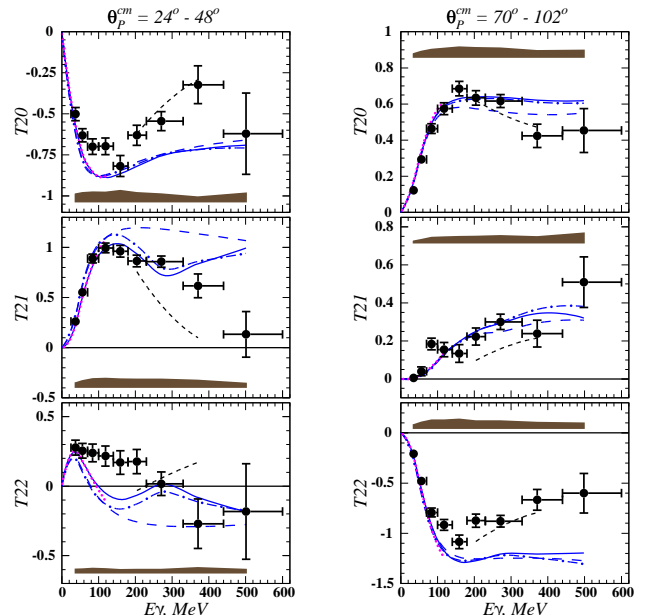


FIG. 4: (color online). Tensor analyzing powers vs. photon energy. Vertical bars are statistical uncertainties; horizontal bars indicate the bin size. Shaded bands show systematic uncertainties. Theoretical predictions are from Arenhövel [7] "N+MEC" (blue long-dashed line), "N+MEC+IC" (blue dash-dotted line), and "N+MEC+IC+RC" (solid line) models, from Levchuk [8] (magenta dotted line), and from Schwamb [10] (black short-dashed line).

tion of the polarization data, which is a difficult test for theory. As both calculations are grounded in fits to nucleon-nucleon and meson photoproduction data, one would hope that the refinements in theory over time and the improvements in the description of the underlying reactions would lead to a clear improvement in all the deuteron PD data, but this is not the case. The pattern of agreement between theory and experiment is similar to that seen for other polarization observables such as  $p_y$  and  $\Sigma$ ; the quality of the agreement decreases at higher energies.

In summary, a new measurement of tensor analyzing powers  $T_{20}$ ,  $T_{21}$  and  $T_{22}$  in deuteron photodisintegration, substantially enhancing the quality and kinematic span of the existing experimental data, has been performed. This enable an accurate test of available models. Theoretical calculations provide an excellent description of these polarization data below pion production threshold, while above pion production threshold a very good description of  $T_{20}$  and  $T_{22}$  is demonstrated by a novel approach incorporating a  $\pi$ -MEC retardation mechanism. The remaining discrepancies could reflect the theoretical uncertainties or some missing or poorly modeled underlying dynamics.

We gratefully acknowledge the staff of VEPP-3 accelerator facility for excellent performance of the ring during the data taking. We are grateful to H.Arenhövel, M.Levchuk and M.Schwamb for useful discussions and for providing us with the results of their calculations. This work was supported in part by Russian Foundation for Basic Research, grants 01-02-

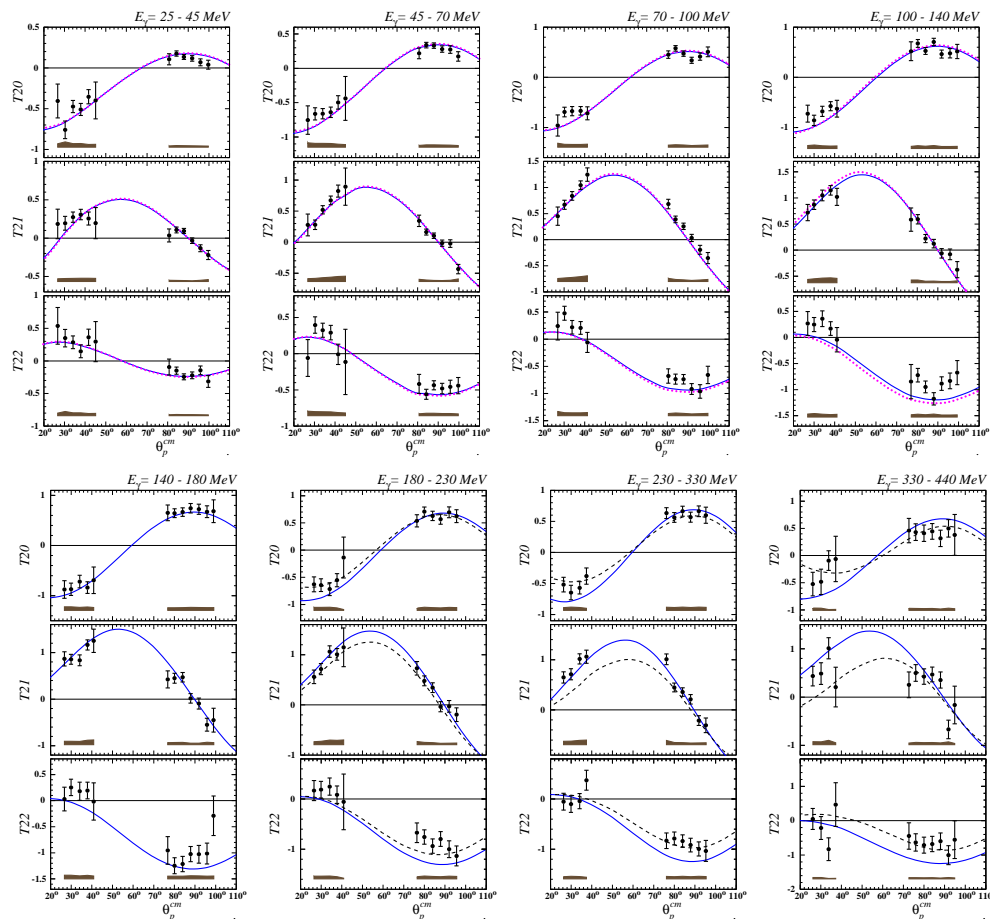


FIG. 5: (color online) Tensor analyzing powers vs. proton emission angle for eight  $E_\gamma$ -bins. Each  $\theta_p^{cm}$  bin is  $4^\circ$  wide. See Fig.4 for notation.

16929, 04-02-16434, 05-02-17080 and 05-02-17688, the U.S. Department of Energy, Office of Nuclear Physics, under con-

tract no. W-31-109-ENG-38, and the U.S. National Science Foundation, grant PHY-03-54871.

- [1] R. Gilman and F. Gross, J. Phys. **G28**, R37 (2002).  
 [2] M.V. Mostovoy, *et al.*, Phys. Lett. **B189**, 181 (1987).  
 [3] K.H.Althoff *et al.*, Z Phys. **C43**, 375 (1989).  
 [4] S.I. Mishnev, *et al.*, Phys. Lett. **B302**, 23 (1993).  
 [5] M.V. Dyug *et al.*, Nucl. Instrum. Methods **A495**, 8 (2002).  
 [6] M.V. Dyug *et al.*, Nucl. Instrum. Methods **A536**, 344 (2005).  
 [7] K.-M. Schmitt and H. Arenhövel, Few-Body Syst. 7, 95 (1989), H.Arenhövel and M. Sanzone, Few-Body Syst. Suppl. 3, 1 (1991), F. Ritz, H. Arenhövel, and T. Wilbois, Few-Body Syst. 24, 123 (1998)  
 [8] M.I. Levchuk, Few-Body Syst. **19**, 77 (1995) and private com-

munication.

- [9] M. Schwamb, H. Arenhövel, Nucl. Phys. **A 690**, 647 (2001), and Nucl. Phys. **A 696**, 556 (2001)  
 [10] M. Schwamb, habilitation thesis, Johannes Gutenberg-Universität at Mainz, 2006  
 [11] <http://www.inp.nsk.su/~rachek/photodisintegration.html>  
 [12] Note that the data from [4] were corrected by re-analysis of the target polarimeter data, resulting in a target polarization  $P_{zz} = 0.48$  instead of  $P_{zz} = 0.58$  used in [4].